



Muons in air showers at the Pierre Auger Observatory: Mean number in highly inclined events

A. Aab,⁴² P. Abreu,⁶⁴ M. Aglietta,⁵³ E. J. Ahn,⁸¹ I. Al Samarai,²⁹ I. F. M. Albuquerque,¹⁷ I. Allekotte,¹ J. Allen,⁸⁵ P. Allison,⁸⁷ A. Almela,^{11,8} J. Alvarez Castillo,⁵⁷ J. Alvarez-Muñiz,⁷⁴ R. Alves Batista,⁴¹ M. Ambrosio,⁴⁴ A. Aminaei,⁵⁸ L. Anchordoqui,^{93,80} S. Andringa,⁶⁴ C. Aramo,⁴⁴ V. M. Aranda,⁷¹ F. Arqueros,⁷¹ H. Asorey,¹ P. Assis,⁶⁴ J. Aublin,³¹ M. Ave,¹ M. Avenier,³² G. Avila,¹⁰ A. M. Badescu,⁶⁸ K. B. Barber,¹² J. Bäumli,³⁶ C. Baus,³⁶ J. J. Beatty,⁸⁷ K. H. Becker,³⁵ J. A. Bellido,¹² C. Berat,³² M. E. Bertaina,⁵³ X. Bertou,¹ P. L. Biermann,³⁹ P. Billoir,³¹ M. Blanco,³¹ C. Bleve,³⁵ H. Blümer,^{36,37} M. Boháčová,²⁷ D. Boncioli,⁵² C. Bonifazi,²³ R. Bonino,⁵³ N. Borodai,⁶² J. Brack,⁷⁸ I. Brancus,⁶⁵ P. Brogueira,⁶⁴ W. C. Brown,⁷⁹ P. Buchholz,⁴² A. Bueno,⁷³ S. Buitink,⁵⁸ M. Buscemi,⁴⁴ K. S. Caballero-Mora,⁵⁵ B. Caccianiga,⁴³ L. Caccianiga,³¹ M. Candusso,⁴⁵ L. Caramete,³⁹ R. Caruso,⁴⁶ A. Castellina,⁵³ G. Cataldi,⁴⁸ L. Cazon,⁶⁴ R. Cester,⁴⁷ A. G. Chavez,⁵⁶ A. Chiavassa,⁵³ J. A. Chinellato,¹⁸ J. Chudoba,²⁷ M. Cilmo,⁴⁴ R. W. Clay,¹² G. Cocciolo,⁴⁸ R. Colalillo,⁴⁴ A. Coleman,⁸⁸ L. Collica,⁴³ M. R. Coluccia,⁴⁸ R. Conceição,⁶⁴ F. Contreras,⁹ M. J. Cooper,¹² A. Cordier,³⁰ S. Coutu,⁸⁸ C. E. Covault,⁷⁶ J. Cronin,⁸⁹ A. Curutiu,³⁹ R. Dallier,^{34,33} B. Daniel,¹⁸ S. Dasso,^{5,3} K. Daumiller,³⁷ B. R. Dawson,¹² R. M. de Almeida,²⁴ M. De Domenico,⁴⁶ S. J. de Jong,^{58,60} J. R. T. de Mello Neto,²³ I. De Mitri,⁴⁸ J. de Oliveira,²⁴ V. de Souza,¹⁶ L. del Peral,⁷² O. Deligny,²⁹ H. Dembinski,³⁷ N. Dhital,⁸⁴ C. Di Giulio,⁴⁵ A. Di Matteo,⁴⁹ J. C. Diaz,⁸⁴ M. L. Díaz Castro,¹⁸ F. Diogo,⁶⁴ C. Dobrigkeit,¹⁸ W. Docters,⁵⁹ J. C. D'Olivo,⁵⁷ A. Dorofeev,⁷⁸ Q. Dorosti Hasankiadeh,³⁷ M. T. Dova,⁴ J. Ebr,²⁷ R. Engel,³⁷ M. Erdmann,⁴⁰ M. Erfani,⁴² C. O. Escobar,^{81,18} J. Espadanal,⁶⁴ A. Etchegoyen,^{8,11} P. Facal San Luis,⁸⁹ H. Falcke,^{58,61,60} K. Fang,⁸⁹ G. Farrar,⁸⁵ A. C. Fauth,¹⁸ N. Fazzini,⁸¹ A. P. Ferguson,⁷⁶ M. Fernandes,²³ B. Fick,⁸⁴ J. M. Figueira,⁸ A. Filevich,⁸ A. Filipčič,^{69,70} B. D. Fox,⁹⁰ O. Fratu,⁶⁸ U. Fröhlich,⁴² B. Fuchs,³⁶ T. Fujii,⁸⁹ R. Gaior,³¹ B. García,⁷ S. T. Garcia Roca,⁷⁴ D. Garcia-Gamez,³⁰ D. Garcia-Pinto,⁷¹ G. Garilli,⁴⁶ A. Gascon Bravo,⁷³ F. Gate,³⁴ H. Gemmeke,³⁸ P. L. Ghia,³¹ U. Giaccari,²³ M. Giammarchi,⁴³ M. Giller,⁶³ C. Glaser,⁴⁰ H. Glass,⁸¹ M. Gómez Berisso,¹ P. F. Gómez Vitale,¹⁰ P. Gonçalves,⁶⁴ J. G. Gonzalez,³⁶ N. González,⁸ B. Gookin,⁷⁸ J. Gordon,⁸⁷ A. Gorgi,⁵³ P. Gorham,⁹⁰ P. Gouffon,¹⁷ S. Grebe,^{58,60} N. Griffith,⁸⁷ A. F. Grillo,⁵² T. D. Grubb,¹² Y. Guardincerri,³ F. Guarino,⁴⁴ G. P. Guedes,¹⁹ M. R. Hampel,⁸ P. Hansen,⁴ D. Harari,¹ T. A. Harrison,¹² S. Hartmann,⁴⁰ J. L. Harton,⁷⁸ A. Haungs,³⁷ T. Hebbeker,⁴⁰ D. Heck,³⁷ P. Heimann,⁴² A. E. Herve,³⁷ G. C. Hill,¹² C. Hojvat,⁸¹ N. Hollon,⁸⁹ E. Holt,³⁷ P. Homola,^{42,62} J. R. Hörandel,^{58,60} P. Horvath,²⁸ M. Hrabovský,^{28,27} D. Huber,³⁶ T. Huege,³⁷ A. Insolia,⁴⁶ P. G. Isar,⁶⁶ K. Islo,⁹³ I. Jandt,³⁵ S. Jansen,^{58,60} C. Jarne,⁴ M. Josebachuili,⁸ A. Kääpä,³⁵ O. Kambeitz,³⁶ K. H. Kampert,³⁵ P. Kasper,⁸¹ I. Katkov,³⁶ B. Kégl,³⁰ B. Keilhauer,³⁷ A. Keivani,⁸⁸ E. Kemp,¹⁸ R. M. Kieckhafer,⁸⁴ H. O. Klages,³⁷ M. Kleifges,³⁸ J. Kleinfeller,⁹ R. Krause,⁴⁰ N. Krohm,³⁵ O. Krömer,³⁸ D. Kruppke-Hansen,³⁵ D. Kuempel,⁴⁰ N. Kunka,³⁸ D. LaHurd,⁷⁶ L. Latronico,⁵³ R. Lauer,⁹² M. Lauscher,⁴⁰ P. Lautridou,³⁴ S. Le Coz,³² M. S. A. B. Leão,¹⁴ D. Lebrun,³² P. Lebrun,⁸¹ M. A. Leigui de Oliveira,²² A. Letessier-Selvon,³¹ I. Lhenry-Yvon,²⁹ K. Link,³⁶ R. López,⁵⁴ K. Louedec,³² J. Lozano Bahilo,⁷³ L. Lu,^{35,75} A. Lucero,⁸ M. Ludwig,³⁶ M. Malacari,¹² S. Maldera,⁵³ M. Mallamaci,⁴³ J. Maller,³⁴ D. Mandat,²⁷ P. Mantsch,⁸¹ A. G. Mariazzi,⁴ V. Marin,³⁴ I. C. Mariş,⁷³ G. Marsella,⁴⁸ D. Martello,⁴⁸ L. Martin,^{34,33} H. Martinez,⁵⁵ O. Martínez Bravo,⁵⁴ D. Martraire,²⁹ J. J. Masías Meza,³ H. J. Mathes,³⁷ S. Mathys,³⁵ J. J. Matthews,⁹² A. J. Matthews,⁸³ G. Matthiae,⁴⁵ D. Maurel,³⁶ D. Maurizio,¹³ E. Mayotte,⁷⁷ P. O. Mazur,⁸¹ C. Medina,⁷⁷ G. Medina-Tanco,⁵⁷ M. Melissas,³⁶ D. Melo,⁸ A. Menshikov,³⁸ S. Messina,⁵⁹ R. Meyhandan,⁹⁰ S. Mićanović,²⁵ M. I. Micheletti,⁶ L. Middendorf,⁴⁰ I. A. Minaya,⁷¹ L. Miramonti,⁴³ B. Mitrica,⁶⁵ L. Molina-Bueno,⁷³ S. Mollerach,¹ M. Monasor,⁸⁹ D. Monnier Ragainne,³⁰ F. Montanet,³² C. Morello,⁵³ M. Mostafá,⁸⁸ C. A. Moura,²² M. A. Muller,^{18,21} G. Müller,⁴⁰ M. Münchmeyer,³¹ R. Mussa,⁴⁷ G. Navarra,^{53,*} S. Navas,⁷³ P. Necasal,²⁷ L. Nellen,⁵⁷ A. Nelles,^{58,60} J. Neuser,³⁵ D. Newton,^{74,75} M. Niechciol,⁴² L. Niemietz,³⁵ T. Niggemann,⁴⁰ D. Nitz,⁸⁴ D. Nosek,²⁶ V. Novotny,²⁶ L. Nožka,²⁸ L. Ochilo,⁴² A. Olinto,⁸⁹ M. Oliveira,⁶⁴ V. M. Olmos-Gilbaja,⁷⁴ N. Pacheco,⁷² D. Pakk Selmi-Dei,¹⁸ M. Palatka,²⁷ J. Pallotta,² N. Palmieri,³⁶ P. Papenbreer,³⁵ G. Parente,⁷⁴ A. Parra,⁵⁴ T. Paul,^{93,86} M. Pech,²⁷ J. Pękala,⁶² R. Pelayo,⁵⁴ I. M. Pepe,²⁰ L. Perrone,⁴⁸ E. Petermann,⁹¹ C. Peters,⁴⁰ S. Petrera,^{49,50} Y. Petrov,⁷⁸ J. Phuntsok,⁸⁸ R. Piegaiá,³ T. Pierog,³⁷ P. Pieroni,³ M. Pimenta,⁶⁴ V. Pirronello,⁴⁶ M. Platino,⁸ M. Plum,⁴⁰ A. Porcelli,³⁷ C. Porowski,⁶² R. R. Prado,¹⁶ P. Privitera,⁸⁹ M. Prouza,²⁷ V. Purrello,¹ E. J. Quel,² S. Quercfeld,³⁵ S. Quinn,⁷⁶ J. Rautenberg,³⁵ O. Ravel,³⁴ D. Ravnigani,⁸ B. Revenu,³⁴ J. Ridky,²⁷ S. Riggi,^{51,74} M. Risse,⁴² P. Ristori,² V. Rizi,⁴⁹ J. Roberts,⁸⁵ W. Rodrigues de Carvalho,⁷⁴ G. Rodriguez Fernandez,⁴⁵ J. Rodriguez Rojo,⁹ M. D. Rodríguez-Frías,⁷² G. Ros,⁷² J. Rosado,⁷¹ T. Rossler,²⁸ M. Roth,³⁷ E. Roulet,¹ A. C. Rovero,⁵ S. J. Saffi,¹² A. Saftoiu,⁶⁵ F. Salamida,²⁹ H. Salazar,⁵⁴ A. Saleh,⁷⁰ F. Salesa Greus,⁸⁸ G. Salina,⁴⁵ F. Sánchez,⁸ P. Sanchez-Lucas,⁷³ C. E. Santo,⁶⁴ E. Santos,¹⁸ E. M. Santos,¹⁷ F. Sarazin,⁷⁷ B. Sarkar,³⁵ R. Sarmiento,⁶⁴ R. Sato,⁹ N. Scharf,⁴⁰ V. Scherini,⁴⁸ H. Schieler,³⁷ P. Schiffer,⁴¹ O. Scholten,⁵⁹ H. Schoorlemmer,^{90,58,60} P. Schovánek,²⁷ F. G. Schröder,^{37,8} A. Schulz,³⁷ J. Schulz,⁵⁸ J. Schumacher,⁴⁰ S. J. Sciutto,⁴ A. Segreto,⁵¹ M. Settimo,³¹ A. Shadkam,⁸³ R. C. Shellard,¹³ I. Sidelnik,¹ G. Sigl,⁴¹ O. Sima,⁶⁷ A. Śmiałkowski,⁶³ R. Šmída,³⁷ G. R. Snow,⁹¹ P. Sommers,⁸⁸ J. Sorokin,¹² R. Squartini,⁹ Y. N. Srivastava,⁸⁶ S. Stanić,⁷⁰ J. Stapleton,⁸⁷ J. Stasielak,⁶² M. Stephan,⁴⁰ A. Stutz,³² F. Suarez,⁸ T. Suomijärvi,²⁹

A. D. Supanitsky,⁵ M. S. Sutherland,⁸⁷ J. Swain,⁸⁶ Z. Szadkowski,⁶³ M. Szuba,³⁷ O. A. Taborda,¹ A. Tapia,⁸ M. Tartare,³² A. Tepe,⁴² V. M. Theodoro,¹⁸ C. Timmermans,^{60,58} C. J. Todero Peixoto,¹⁵ G. Toma,⁶⁵ L. Tomankova,³⁷ B. Tomé,⁶⁴ A. Tonachini,⁴⁷ G. Torralba Elipe,⁷⁴ D. Torres Machado,²³ P. Travnicek,²⁷ E. Trovato,⁴⁶ R. Ulrich,³⁷ M. Unger,³⁷ M. Urban,⁴⁰ J. F. Valdés Galicia,⁵⁷ I. Valiño,⁷⁴ L. Valore,⁴⁴ G. van Aar,⁵⁸ A. M. van den Berg,⁵⁹ S. van Velzen,⁵⁸ A. van Vliet,⁴¹ E. Varela,⁵⁴ B. Vargas Cárdenas,⁵⁷ G. Varner,⁹⁰ J. R. Vázquez,⁷¹ R. A. Vázquez,⁷⁴ D. Veberič,³⁰ V. Verzi,⁴⁵ J. Vicha,²⁷ M. Videla,⁸ L. Villaseñor,⁵⁶ B. Vlcek,⁹³ S. Vorobiov,⁷⁰ H. Wahlberg,⁴ O. Wainberg,^{8,11} D. Walz,⁴⁰ A. Watson,⁷⁵ M. Weber,³⁸ K. Weidenhaupt,⁴⁰ A. Weindl,³⁷ F. Werner,³⁶ A. Widom,⁸⁶ L. Wiencke,⁷⁷ B. Wilczyńska,^{62,*} H. Wilczyński,⁶² M. Will,³⁷ C. Williams,⁸⁹ T. Winchen,³⁵ D. Wittkowski,³⁵ B. Wundheiler,⁸ S. Wykes,⁵⁸ T. Yamamoto,^{89,†} T. Yapici,⁸⁴ P. Younk,⁸² G. Yuan,⁸³ A. Yushkov,⁴² B. Zamorano,⁷³ E. Zas,⁷⁴ D. Zavrtanik,^{70,69} M. Zavrtanik,^{69,70} I. Zaw,^{85,§} A. Zepeda,^{55,‡} J. Zhou,⁸⁹ Y. Zhu,³⁸ M. Zimbres Silva,¹⁸ M. Ziolkowski,⁴² and F. Zuccarello⁴⁶

(Pierre Auger Collaboration)

¹*Centro Atómico Bariloche and Instituto Balseiro (CNEA-UNCuyo-CONICET),
San Carlos de Bariloche, Argentina*

²*Centro de Investigaciones en Láseres y Aplicaciones, CITEDEF and CONICET, Argentina*

³*Departamento de Física, FCEyN, Universidad de Buenos Aires y CONICET, Argentina*

⁴*IFLP, Universidad Nacional de La Plata and CONICET, La Plata, Argentina*

⁵*Instituto de Astronomía y Física del Espacio (CONICET-UBA), Buenos Aires, Argentina*

⁶*Instituto de Física de Rosario (IFIR) - CONICET/U.N.R. and Facultad de Ciencias Bioquímicas y
Farmacéuticas U.N.R., Rosario, Argentina*

⁷*Instituto de Tecnologías en Detección y Astropartículas (CNEA, CONICET, UNSAM),
and National Technological University, Faculty Mendoza (CONICET/CNEA), Mendoza, Argentina*

⁸*Instituto de Tecnologías en Detección y Astropartículas (CNEA, CONICET, UNSAM),
Buenos Aires, Argentina*

⁹*Observatorio Pierre Auger, Malargüe, Argentina*

¹⁰*Observatorio Pierre Auger and Comisión Nacional de Energía Atómica, Malargüe, Argentina*

¹¹*Universidad Tecnológica Nacional - Facultad Regional Buenos Aires,
Buenos Aires, Argentina*

¹²*University of Adelaide, Adelaide, S.A., Australia*

¹³*Centro Brasileiro de Pesquisas Físicas, Rio de Janeiro, RJ, Brazil*

¹⁴*Faculdade Independente do Nordeste, Vitória da Conquista, Brazil*

¹⁵*Universidade de São Paulo, Escola de Engenharia de Lorena, Lorena, SP, Brazil*

¹⁶*Universidade de São Paulo, Instituto de Física de São Carlos, São Carlos, SP, Brazil*

¹⁷*Universidade de São Paulo, Instituto de Física, São Paulo, SP, Brazil*

¹⁸*Universidade Estadual de Campinas, IFGW, Campinas, SP, Brazil*

¹⁹*Universidade Estadual de Feira de Santana, Brazil*

²⁰*Universidade Federal da Bahia, Salvador, BA, Brazil*

²¹*Universidade Federal de Pelotas, Pelotas, RS, Brazil*

²²*Universidade Federal do ABC, Santo André, SP, Brazil*

²³*Universidade Federal do Rio de Janeiro, Instituto de Física, Rio de Janeiro, RJ, Brazil*

²⁴*Universidade Federal Fluminense, EEIMVR, Volta Redonda, RJ, Brazil*

²⁵*Rudjer Bošković Institute, 10000 Zagreb, Croatia*

²⁶*Charles University, Faculty of Mathematics and Physics, Institute of Particle and Nuclear Physics,
Prague, Czech Republic*

²⁷*Institute of Physics of the Academy of Sciences of the Czech Republic, Prague, Czech Republic*

²⁸*Palacky University, RCPTM, Olomouc, Czech Republic*

²⁹*Institut de Physique Nucléaire d'Orsay (IPNO), Université Paris 11, CNRS-IN2P3, Orsay, France*

³⁰*Laboratoire de l'Accélérateur Linéaire (LAL), Université Paris 11, CNRS-IN2P3, France*

³¹*Laboratoire de Physique Nucléaire et de Hautes Energies (LPNHE),
Universités Paris 6 et Paris 7, CNRS-IN2P3, Paris, France*

³²*Laboratoire de Physique Subatomique et de Cosmologie (LPSC), Université Grenoble-Alpes,
CNRS-IN2P3, France*

³³*Station de Radioastronomie de Nançay, Observatoire de Paris, CNRS/INSU, France*

³⁴*SUBATECH, École des Mines de Nantes, CNRS-IN2P3, Université de Nantes, France*

³⁵*Bergische Universität Wuppertal, Wuppertal, Germany*

³⁶*Karlsruhe Institute of Technology - Campus South - Institut für Experimentelle Kernphysik (IEKP),
Karlsruhe, Germany*

³⁷*Karlsruhe Institute of Technology - Campus North - Institut für Kernphysik,
Karlsruhe, Germany*

- ³⁸Karlsruhe Institute of Technology - Campus North - Institut für Prozessdatenverarbeitung und Elektronik, Karlsruhe, Germany
- ³⁹Max-Planck-Institut für Radioastronomie, Bonn, Germany
- ⁴⁰RWTH Aachen University, III. Physikalisches Institut A, Aachen, Germany
- ⁴¹Universität Hamburg, Hamburg, Germany
- ⁴²Universität Siegen, Siegen, Germany
- ⁴³Università di Milano and Sezione INFN, Milan, Italy
- ⁴⁴Università di Napoli “Federico II” and Sezione INFN, Napoli, Italy
- ⁴⁵Università di Roma II “Tor Vergata” and Sezione INFN, Roma, Italy
- ⁴⁶Università di Catania and Sezione INFN, Catania, Italy
- ⁴⁷Università di Torino and Sezione INFN, Torino, Italy
- ⁴⁸Dipartimento di Matematica e Fisica “E. De Giorgi” dell’Università del Salento and Sezione INFN, Lecce, Italy
- ⁴⁹Dipartimento di Scienze Fisiche e Chimiche dell’Università dell’Aquila and INFN, Italy
- ⁵⁰Gran Sasso Science Institute (INFN), L’Aquila, Italy
- ⁵¹Istituto di Astrofisica Spaziale e Fisica Cosmica di Palermo (INAF), Palermo, Italy
- ⁵²INFN, Laboratori Nazionali del Gran Sasso, Assergi (L’Aquila), Italy
- ⁵³Osservatorio Astrofisico di Torino (INAF), Università di Torino and Sezione INFN, Torino, Italy
- ⁵⁴Benemérita Universidad Autónoma de Puebla, Puebla, Mexico
- ⁵⁵Centro de Investigación y de Estudios Avanzados del IPN (CINVESTAV), México, Mexico
- ⁵⁶Universidad Michoacana de San Nicolas de Hidalgo, Morelia, Michoacan, Mexico
- ⁵⁷Universidad Nacional Autónoma de México, México, D.F., Mexico
- ⁵⁸IMAPP, Radboud University Nijmegen, Netherlands
- ⁵⁹KVI - Center for Advanced Radiation Technology, University of Groningen, Netherlands
- ⁶⁰Nikhef, Science Park, Amsterdam, Netherlands
- ⁶¹ASTRON, Dwingeloo, Netherlands
- ⁶²Institute of Nuclear Physics PAN, Krakow, Poland
- ⁶³University of Łódź, Łódź, Poland
- ⁶⁴Laboratório de Instrumentação e Física Experimental de Partículas - LIP and Instituto Superior Técnico - IST, Universidade de Lisboa - UL, Portugal
- ⁶⁵‘Horia Hulubei’ National Institute for Physics and Nuclear Engineering, Bucharest- Magurele, Romania
- ⁶⁶Institute of Space Sciences, Bucharest, Romania
- ⁶⁷University of Bucharest, Physics Department, Romania
- ⁶⁸University Politehnica of Bucharest, Romania
- ⁶⁹Experimental Particle Physics Department, J. Stefan Institute, Ljubljana, Slovenia
- ⁷⁰Laboratory for Astroparticle Physics, University of Nova Gorica, Slovenia
- ⁷¹Universidad Complutense de Madrid, Madrid, Spain
- ⁷²Universidad de Alcalá, Alcalá de Henares (Madrid), Spain
- ⁷³Universidad de Granada and C.A.F.P.E., Granada, Spain
- ⁷⁴Universidad de Santiago de Compostela, Spain
- ⁷⁵School of Physics and Astronomy, University of Leeds, United Kingdom
- ⁷⁶Case Western Reserve University, Cleveland, OH 44106, USA
- ⁷⁷Colorado School of Mines, Golden, CO 80401, USA
- ⁷⁸Colorado State University, Fort Collins, CO 80523, USA
- ⁷⁹Colorado State University, Pueblo, CO 81001, USA
- ⁸⁰Department of Physics and Astronomy, Lehman College, City University of New York, New York, NY 10468, USA
- ⁸¹Fermilab, Batavia, IL 60510-0500, USA
- ⁸²Los Alamos National Laboratory, Los Alamos, NM 87545, USA
- ⁸³Louisiana State University, Baton Rouge, LA 70803-4001, USA
- ⁸⁴Michigan Technological University, Houghton, MI 49931-1295, USA
- ⁸⁵New York University, New York, NY 10003, USA
- ⁸⁶Northeastern University, Boston, MA 02115-5096, USA
- ⁸⁷Ohio State University, Columbus, OH 43210-1061, USA
- ⁸⁸Pennsylvania State University, University Park, PA 16802-6300, USA
- ⁸⁹University of Chicago, Enrico Fermi Institute, Chicago, IL 60637, USA
- ⁹⁰University of Hawaii, Honolulu, HI 96822, USA
- ⁹¹University of Nebraska, Lincoln, NE 68588-0111, USA

⁹²*University of New Mexico, Albuquerque, NM 87131, USA*⁹³*University of Wisconsin, Milwaukee, WI 53201, USA*

(Received 13 August 2014; published 6 February 2015)

We present the first hybrid measurement of the average muon number in air showers at ultrahigh energies, initiated by cosmic rays with zenith angles between 62° and 80° . The measurement is based on 174 hybrid events recorded simultaneously with the surface detector array and the fluorescence detector of the Pierre Auger Observatory. The muon number for each shower is derived by scaling a simulated reference profile of the lateral muon density distribution at the ground until it fits the data. A 10^{19} eV shower with a zenith angle of 67° , which arrives at the surface detector array at an altitude of 1450 m above sea level, contains on average $(2.68 \pm 0.04 \pm 0.48(\text{sys})) \times 10^7$ muons with energies larger than 0.3 GeV. The logarithmic gain $d \ln N_\mu / d \ln E$ of muons with increasing energy between 4×10^{18} eV and 5×10^{19} eV is measured to be $(1.029 \pm 0.024 \pm 0.030(\text{sys}))$.

DOI: [10.1103/PhysRevD.91.032003](https://doi.org/10.1103/PhysRevD.91.032003)

PACS numbers: 96.50.sd, 13.85.Tp, 98.70.Sa

I. INTRODUCTION

Understanding the mass composition of ultrahigh energy cosmic rays at Earth is fundamental to unveil their production and propagation mechanisms. The interpretation of observed anisotropies [1,2] and of features in the flux relies on it, such as the break in the power law spectrum around 4×10^{18} eV, and the flux suppression above 4×10^{19} eV [3].

Ultrahigh energy cosmic rays can only be observed indirectly through air showers. The mass composition of cosmic rays can be derived from certain air shower observables, but the inference is limited by our theoretical understanding of the air shower development [4]. Air shower simulations require knowledge of hadronic interaction properties at very high energies and in phase space regions that are not well covered by accelerator experiments. The systematic uncertainty of the inferred mass composition can be reduced by studying different observables (see, e.g., [5]). The slant depth X_{max} of the shower maximum is a prominent mass-sensitive tracer, since it can be measured directly with fluorescence telescopes.

The number of muons in an air shower is another powerful tracer of the mass. Simulations show that the produced number of muons, N_μ , rises almost linearly with the cosmic-ray energy E , and increases with a small power of the cosmic-ray mass A . This behavior can be understood in terms of the generalized Heitler model of hadronic air showers [6], which predicts

$$N_\mu = A \left(\frac{E/A}{\xi_c} \right)^\beta, \quad (1)$$

where ξ_c is the critical energy at which charged pions decay into muons and $\beta \approx 0.9$. Detailed simulations show further

dependencies on hadronic-interaction properties, like the multiplicity, the charge ratio and the baryon antibaryon pair production [7,8].

To use the muon number N_μ as a tracer for the mass A , the cosmic-ray energy E has to be independently measured event by event with a small systematic uncertainty. By taking the logarithm of Eq. (1) and computing the derivative, we obtain the logarithmic gain of muons with increasing energy

$$\frac{d \ln N_\mu}{d \ln E} = \beta + (1 - \beta) \frac{d \ln A}{d \ln E}, \quad (2)$$

which carries additional information on the changes in the mass composition and is invariant to systematic offsets in the energy scale. The dependency of the muon number N_μ on the mass of cosmic rays is complementary to other mass-sensitive observables such as the depth of the shower maximum, X_{max} . If both observables are combined, the internal consistency of hadronic interaction models can be tested.

We present the average number of muons in inclined showers above 4×10^{18} eV measured with the Pierre Auger Observatory [9], which is located in Mendoza province, Argentina. The Pierre Auger Observatory was completed in 2008 and covers an area of 3000 km². It is a hybrid instrument to detect cosmic-ray induced air showers, which combines a surface detector array (SD) of 1660 water-Cherenkov stations [10] placed on a triangular grid with 1.5 km spacing with a fluorescence detector (FD) [11]. Due to their cylindrical volume, the surface detectors are sensitive to inclined and even horizontal particles [12,13]. On dark nights, which correspond to a duty cycle of about 13%, the longitudinal shower development and the calorimetric energy of the shower are measured by the FD. It consists of 27 telescopes with UV filters located at four sites around the SD array, each monitoring a $30^\circ \times 28^\circ$ patch of the sky.

*Deceased.

†Now at Konan University.

‡Also at the Universidad Autonoma de Chiapas on leave of absence from Cinvestav.

§Now at NYU Abu Dhabi.

Extensive air showers with zenith angles exceeding 62° are characterized at the ground by the dominance of secondary energetic muons, since the electromagnetic component has been largely absorbed in the large atmospheric depth crossed by the shower. Such inclined showers provide a direct measurement of the muon number at the ground [14]. The muon number in less inclined air showers has also been explored [15,16], but the measurement is in this case complicated by the need to separate the electromagnetic and the muonic signals in surface detectors. The unique features of showers around 60° zenith angle further led to the derivation of the muon production depth from the arrival times of signals in the SD [17], which is another powerful observable to study the mass composition and hadronic interaction models.

We measure the muon number in inclined air showers using the relative scale factor N_{19} which relates the observed muon densities at the ground to the average muon density profile of simulated proton-induced air showers of fixed energy 10^{19} eV. This approach follows from developments that have been introduced to reconstruct inclined showers, taking into account the rich spatial structure of the muon distributions at the ground. The scale factor N_{19} is independent of the zenith angle and details of the location of the observatory [18,19] and can be also used as an estimator of the muon number. These developments led to the first limit on the fraction of cosmic photons in the EeV energy range [20] and to an independent measurement of the energy spectrum of cosmic rays [21].

II. RECONSTRUCTION OF THE MUON NUMBER

Inclined showers generate asymmetric and elongated signal patterns in the SD array with narrow pulses in time, typical for a muonic shower front. Events are selected by demanding space-time coincidences of the signals of triggered surface detectors which must be consistent with the arrival of a shower front [10,22]. After event selection, the arrival direction (θ, ϕ) of the cosmic ray is determined from the arrival times of this front at the triggered stations by fitting a model of the shower front propagation. The achieved angular resolution is better than 0.6° above 4×10^{18} eV [23].

Once the shower direction is established, we model the muon density ρ_μ at the ground point \vec{r} as

$$\rho_\mu(\vec{r}) = N_{19} \rho_{\mu,19}(\vec{r}; \theta, \phi), \quad (3)$$

where $\rho_{\mu,19}$ is the parametrized ground density for a proton shower simulated at 10^{19} eV with the hadronic interaction model QGSJETII-03 [24]. An example is given in Fig. 1. It was shown in detailed studies [25,26] that the attenuation and shape of $\rho_{\mu,19}$ depend very weakly on the cosmic-ray energy E and mass A for showers with $\theta > 60^\circ$, so the factorization in Eq. (3) is a good approximation for showers

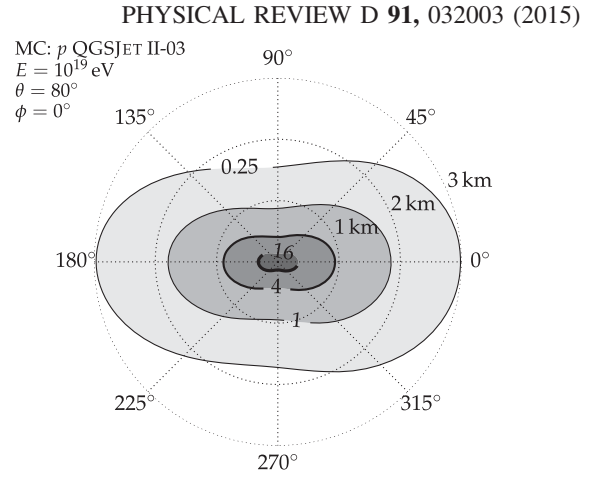


FIG. 1. Expected number of muon hits per SD station as predicted by the reference profile $\rho_{\mu,19}$, for $\theta = 80^\circ$ and $\phi = 0^\circ$, in cylindrical coordinates around the shower axis. The radial density roughly follows a power law in any given direction. The quadrupole structure is generated by charge separation in Earth's magnetic field. The weaker dipole structure is caused by projection effects and muon attenuation. Early (late) arriving particles are on the right (left) side in this projection.

above 10^{18} eV. It was also shown that the lateral shape of $\rho_{\mu,19}$ is consistently reproduced by different hadronic interaction models and air shower simulation codes. The lateral shape at the ground is mainly determined by hadronic interactions at beam energies of up to a few hundred GeV, in which models are constrained by data from fixed target experiments. The strong zenith angle dependence is factorized out into $\rho_{\mu,19}$ in Eq. (3), so that the scale factor N_{19} at a given zenith angle is a relative measure of the produced number of muons N_μ , addressed in Eq. (1).

The scale factor N_{19} is inferred from measured signals with a maximum-likelihood method based on a probabilistic model of the detector response to muon hits obtained from GEANT4 [27] simulations with the Auger Offline software framework [28]. A residual electromagnetic signal component is taken into account based on model predictions (typically amounting to 20% of the muon signal) [29]. The procedure is described in full detail in Ref. [30].

The reconstruction approach was validated in an end-to-end test with three sets of simulated events. The first set consists of 100,000 proton and 100,000 iron showers generated with AIRES [31], using QGSJET01 [32]. Showers following an $E^{-2.6}$ energy spectrum and an isotropic angular distribution were simulated at a relative thinning of 10^{-6} . The second (third) set consists of 12,000 proton and 12,000 iron showers generated using CORSIKA [33], with QGSJETII-04 [34] (EPOS LHC [35]), with the same thinning and angular distribution and an E^{-1} energy spectrum. Showers have subsequently undergone a full simulation of the detector, with random placement of impact points in the SD array. Simulated and real events were reconstructed with the same procedure.

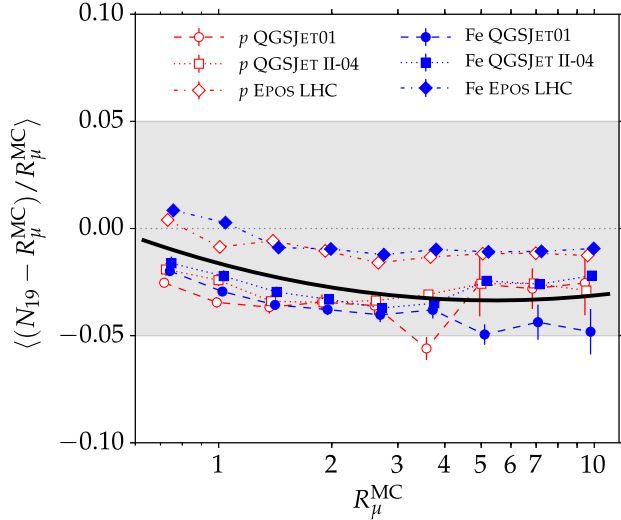


FIG. 2 (color online). Average relative deviation of reconstructed muon content N_{19} from the true muon content R_{μ}^{MC} (as defined in the text) for proton and iron showers. The shaded area indicates the systematic uncertainty of N_{19} . The solid black line represents a second order polynomial adjusted to describe the mean bias.

For each MC event we compute the ratio $R_{\mu}^{\text{MC}} = N_{\mu}/N_{\mu,19}$ by counting the total number of muons N_{μ} at the ground in the simulation and dividing by the total number of muons $N_{\mu,19} = \int dy \int \rho_{\mu,19} dx$ obtained by integrating the reference model. We compare this ratio with the value of N_{19} obtained from the fit of Eq. (3).

The relative deviation of N_{19} from R_{μ}^{MC} is shown in Fig. 2 to be within 5% for events with $R_{\mu}^{\text{MC}} > 0.6$. This confirms the factorization hypothesis of Eq. (3), the approximate universality of the chosen reference profile and validates the reconstruction method. The largest source of systematic bias is the remaining model dependence of the reference profile $\rho_{\mu,19}(\vec{r})$. To get an unbiased estimator, we correct the measured value N_{19} for the average bias. We use a second order polynomial as indicated in Fig. 2 to reproduce R_{μ}^{MC} to within 3% for the latest models. We consequently call the corrected estimator R_{μ} in the following.

We constructed in this way an unbiased estimator of the total number of muons at the ground that is nearly independent of model assumptions and the zenith angle of the shower. The value $R_{\mu} = 1$ corresponds to 2.148×10^7 (1.202×10^7 , 5.223×10^6) muons with energies above 0.3 GeV (Cherenkov threshold for muons in water) that reach the Auger site at an altitude¹ of 1425 m at a shower inclination of 60° (70° , 80°). By combining the model uncertainty with that of the simulated muon response of the

¹Altitudes are given with respect to the WGS 84 reference ellipsoid [36].

detectors at $\theta > 60^{\circ}$ [37], we conservatively estimate the systematic uncertainty of R_{μ} to be 11%.

III. DATA SET AND EVENT SELECTION

We proceed to study the muon content R_{μ} of inclined showers as a function of the cosmic-ray energy E . The calorimetric energy E_{cal} of the shower is measured independently by the FD in a subset of hybrid events recorded simultaneously in FD and SD. The total energy E is computed by adding the average invisible energy $\langle E_{\text{inv}} \rangle$, which has been re-evaluated recently based on data [38]. Since R_{μ} is sensitive to the cosmic-ray mass A , we make sure not to bias the selected sample towards certain masses by a careful selection of the accepted shower geometries.

The data set consists of hybrid events with zenith angles $62^{\circ} < \theta < 80^{\circ}$ and at least four triggered stations. Only events well contained in the SD array are considered; the station closest to the fitted core and its six adjacent stations need all be active. The FD measurements have to pass quality cuts designed to ensure an accurate reconstruction of arrival direction and longitudinal profile. The cuts are adapted versions of those used in calibration of events with $\theta < 60^{\circ}$ [39]. The SD station used in the FD geometrical reconstruction must be closer to the core than 750 m. Only events with good atmospheric conditions are considered: the vertical aerosol optical depth needs to be measured and has to be less than 0.1; if cloud information is available we require a cloud coverage below 25% in the field of view, a distance from the cloud layer to the measured profile larger than 50 g cm^{-2} , and a thickness of the cloud layer less than 100 g cm^{-2} . The few remaining longitudinal profiles affected by clouds are rejected by requiring a small χ^2 -residual in the Gaisser-Hillas fit, $(\chi^2 - n_{\text{dof}})/\sqrt{2n_{\text{dof}}} < 3$, and the parameter X_0 of the fitted Gaisser-Hillas profile must be negative.

In addition to the quality selection criteria, a fiducial cut on the FD field of view is applied to ensure that it is large enough to observe the depth of shower maximum with equal probability within the range of plausible values. This cut also ensures a maximum accepted uncertainty of the depth of the shower maximum of 150 g cm^{-2} , and a minimum viewing angle of light in the FD telescope of 25° . Finally, we accept only energies above $4 \times 10^{18} \text{ eV}$ to ensure a trigger probability of 100% for FD and SD.

The selection is applied to inclined events recorded from 1 January 2004 to 1 January 2013. Out of 29722 hybrid events, 174 events are accepted. Due to the geometrical acceptance of the SD and the fiducial cut on the FD field of view, the zenith angle distribution peaks near 62° . The average zenith angle is $(66.9 \pm 0.3)^{\circ}$ and the highest energy in the sample is $(48.7 \pm 2.9) \times 10^{18} \text{ eV}$.

IV. DATA ANALYSIS

The muon content R_μ of individual showers with the same energy E and arrival direction varies. This is caused by statistical fluctuations in the development of the hadronic cascade, and, in addition, by random sampling from a possibly mixed mass composition. We will refer to these fluctuations combined as intrinsic fluctuations. In the following, we will make statements about the average shower, meaning that the average is taken over these intrinsic fluctuations. Detector sampling adds Gaussian fluctuations to the observed value of R_μ on top of that. The statistical uncertainties of R_μ and E caused by the sampling are estimated by the reconstruction algorithms event by event. We will refer to them as detection uncertainties.

From Eq. (1) we expect that the average number of produced muons, which is proportional to $\langle R_\mu \rangle$, and the cosmic-ray energy E have a relationship that is not far from a power law. Therefore we fit the parametrization

$$\langle R_\mu \rangle = a(E/10^{19} \text{ eV})^b \quad (4)$$

to the selected data set, using a detailed maximum-likelihood method that takes the mentioned fluctuations into account. Intrinsic fluctuations of R_μ are modeled with a normal distribution that has a constant relative standard deviation $\sigma[R_\mu]/R_\mu$. This model is found to be in good agreement with shower simulations. The a parameter of the fitted curve represents the average muon content $\langle R_\mu \rangle(10^{19} \text{ eV})$ at 10^{19} eV and the b parameter the logarithmic gain $d\langle \ln R_\mu \rangle/d \ln E \simeq d \ln N_\mu/d \ln E$ of muons with growing energy. The maximum-likelihood method was validated with a fast realistic simulation of hybrid events and shown to yield unbiased values for a and b . The technical aspects will be presented in a separate paper.

The data and results of the fit are shown in Fig. 3. We obtain

$$a = \langle R_\mu \rangle(10^{19} \text{ eV}) = (1.841 \pm 0.029 \pm 0.324(\text{sys})), \quad (5)$$

$$b = d\langle \ln R_\mu \rangle/d \ln E = (1.029 \pm 0.024 \pm 0.030(\text{sys})), \quad (6)$$

$$\sigma[R_\mu]/R_\mu = (0.136 \pm 0.015 \pm 0.033(\text{sys})). \quad (7)$$

At a zenith angle of 67° , this corresponds to $(2.68 \pm 0.04 \pm 0.48(\text{sys})) \times 10^7$ muons with energies larger than 0.3 GeV that reach 1425 m altitude in an average 10^{19} eV shower.

The fitted model agrees well with data. To obtain a goodness-of-fit estimator, we compute the histogram of the residuals $(R_\mu - \langle R_\mu \rangle)/\langle R_\mu \rangle$ and compare it with its expectation $g((R_\mu - \langle R_\mu \rangle)/\langle R_\mu \rangle) = \int f((R_\mu - \langle R_\mu \rangle)(E))/\langle R_\mu \rangle(E), E dE$ computed from the fitted two-dimensional probability density function $f(R_\mu, E)$. Histogram and expectation are shown in the inset of Fig. 3. The comparison yields a reduced chi-square value $\chi^2/n_{\text{dof}} = 4.9/10$ for the fitted model.

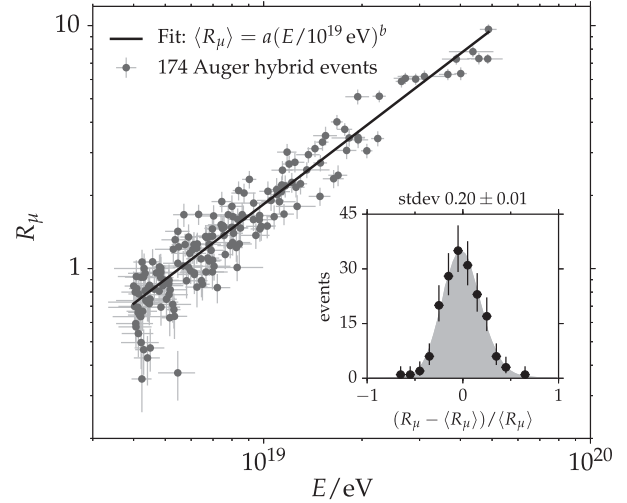


FIG. 3. The selected hybrid events above $4 \times 10^{18} \text{ eV}$ and a fit of the power law $\langle R_\mu \rangle = a(E/10^{19} \text{ eV})^b$. The error bars indicate statistical detection uncertainties only. The inset shows a histogram of the residuals around the fitted curve (black dots) and for comparison the expected residual distribution computed from the fitted probability model that describes the fluctuations.

The systematic uncertainty of the absolute scale $\langle R_\mu \rangle(10^{19} \text{ eV})$ of 18% combines the intrinsic uncertainty of the R_μ -measurement (11%) and the uncertainty of the Auger energy scale (14%) [38]. The systematic uncertainty of the logarithmic gain $d\langle \ln R_\mu \rangle/d \ln E$ of 3% is derived from variations of the FD selection cuts (2%), variations of the bias correction of R_μ within its systematic uncertainty (1%), variations of the distribution assumptions on the intrinsic R_μ -fluctuations (1%) and by assuming a residual zenith-angle dependence of the ratio R_μ/E that cannot be detected within the current statistics (0.5%). The third parameter $\sigma[R_\mu]/R_\mu$, the relative size of the intrinsic fluctuations, is effectively obtained by subtraction of the detection uncertainties from the total spread. Its systematic uncertainty of ± 0.033 is estimated from the variations just described [$\pm 0.014(\text{sys})$ in total], and by varying the detection uncertainties within a plausible range [$\pm 0.030(\text{sys})$].

At $\theta = 67^\circ$, the average zenith angle of the data set, $R_\mu = 1$ corresponds to $N_\mu = 1.455 \times 10^7$ muons at the ground with energies above 0.3 GeV. For model comparisons, it is sufficient to simulate showers at this zenith angle down to an altitude of 1425 m and count muons at the ground with energies above 0.3 GeV. Their number should then be divided by $N_\mu = 1.455 \times 10^7$ to obtain R_μ^{MC} , which can be directly compared to our measurement.

Our fit yields the average muon content $\langle R_\mu \rangle$. For model comparisons the average logarithmic muon content, $\langle \ln R_\mu \rangle$, is also of interest, as we will see in the next section. The relationship between the two depends on shape and size of the intrinsic fluctuations. We compute

$\langle \ln R_\mu \rangle$ numerically based on our fitted model of the intrinsic fluctuations:

$$\begin{aligned} \langle \ln R_\mu \rangle (10^{19} \text{ eV}) &= \int_0^\infty \ln R_\mu \mathcal{N}(R_\mu) dR_\mu \\ &= 0.601 \pm 0.016_{-0.201}^{+0.167} (\text{sys}), \end{aligned} \quad (8)$$

where $\mathcal{N}(R_\mu)$ is a Gaussian with mean $\langle R_\mu \rangle$ and spread $\sigma[R_\mu]$ as obtained from the fit. The deviation of $\langle \ln R_\mu \rangle$ from $\ln \langle R_\mu \rangle$ is only 2% so that the conversion does not lead to a noticeable increase in the systematic uncertainty.

Several consistency checks were performed on the data set. We found no indications for a seasonal variation, or for a dependence on the zenith angle or the distance of the shower axis to the fluorescence telescopes.

V. MODEL COMPARISON AND DISCUSSION

A simple comparison of our data with air showers simulated at the mean zenith angle $\theta = 67^\circ$ with the hadronic interaction models QGSJETII-04 and EPOS LHC is shown in Fig. 4. The ratio $\langle R_\mu \rangle / (E/10^{19} \text{ eV})$ cancels most of the energy scaling, and emphasizes the effect of the cosmic-ray mass A on the muon number. We compute the ratio from Eq. (4) (line), and alternatively by a binwise averaging of the original data (data points). The

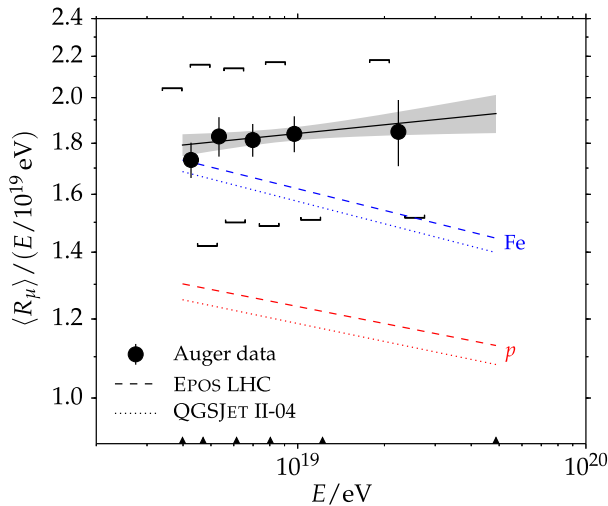


FIG. 4 (color online). Average muon content $\langle R_\mu \rangle$ per shower energy E as a function of the shower energy E in double logarithmic scale. Our data is shown bin by bin (circles) together with the fit discussed in the previous section (line). Square brackets indicate the systematic uncertainty of the measurement; the diagonal offsets represent the correlated effect of systematic shifts in the energy scale. The grey band indicates the statistical uncertainty of the fitted line. Shown for comparison are theoretical curves for proton and iron showers simulated at $\theta = 67^\circ$ (dotted and dashed lines). Black triangles at the bottom show the energy bin edges. The binning was adjusted by an algorithm to obtain equal numbers of events per bin.

two ways of computing the ratio are visually in good agreement, despite minor bin-to-bin migration effects that bias the binwise method. The fitting approach we used for the data analysis avoids the migration bias by design.

Proton and iron showers are well separated, which illustrates the power of $\langle R_\mu \rangle$ as a composition estimator. A caveat is the large systematic uncertainty on the absolute scale of the measurement, which is mainly inherited from the energy scale [38]. This limits its power as a mass composition estimator, but we will see that our measurement contributes valuable insights into the consistency of hadronic interaction models around and above energies of 10^{19} eV, where other sensitive data are sparse.

A hint of a discrepancy between the models and the data is the high abundance of muons in the data. The measured muon number is higher than in pure iron showers, suggesting contributions of even heavier elements. This interpretation is not in agreement with studies based on the depth of shower maximum [40], which show an average logarithmic mass $\langle \ln A \rangle$ between proton and iron in this energy range. We note that our data points can be moved between the proton and iron predictions by shifting them within the systematic uncertainties, but we will demonstrate that this does not completely resolve the discrepancy. The logarithmic gain $d\langle \ln R_\mu \rangle / d \ln E$ of the data is also large compared to proton or iron showers. This suggests a transition from lighter to heavier elements that is also seen in the evolution of the average depth of shower maximum.

We will now quantify the disagreement between model predictions and our data with the help of the mass composition inferred from the average depth $\langle X_{\max} \rangle$ of the shower maximum. A valid hadronic interaction model has to describe all air shower observables consistently. We have recently published the mean logarithmic mass $\langle \ln A \rangle$ derived from the measured average depth of the shower maximum $\langle X_{\max} \rangle$ [40]. We can therefore make predictions for the mean logarithmic muon content $\langle \ln R_\mu \rangle$ based on these $\langle \ln A \rangle$ data, and compare them directly to our measurement.

We consider QGSJET01, QGSJETII-03, QGSJETII-04, and EPOS LHC for this comparison. The relation of $\langle X_{\max} \rangle$ and $\langle \ln A \rangle$ at a given energy E for these models is in good agreement with the prediction from the generalized Heitler model of hadronic air showers,

$$\langle X_{\max} \rangle = \langle X_{\max} \rangle_p + f_E \langle \ln A \rangle, \quad (9)$$

where $\langle X_{\max} \rangle_p$ is the average depth of the shower maximum for proton showers at the given energy and f_E an energy-dependent parameter [4,41]. The parameters $\langle X_{\max} \rangle_p$ and f_E were computed from air shower simulations for each model.

We derive a similar expression from Eq. (1) by substituting $N_{\mu,p} = (E/\xi_c)^\beta$ and computing the average logarithm of the muon number

$$\langle \ln N_\mu \rangle = \langle \ln N_\mu \rangle_p + (1 - \beta) \langle \ln A \rangle \quad (10)$$

$$\beta = 1 - \frac{\langle \ln N_\mu \rangle_{\text{Fe}} - \langle \ln N_\mu \rangle_p}{\ln 56}. \quad (11)$$

Since $N_\mu \propto R_\mu$, we can replace $\ln N_\mu$ by $\ln R_\mu$. The same can be done in Eq. (2), which also holds for averages due to the linearity of differentiation.

We estimate the systematic uncertainty of the approximate Heitler model by computing β from Eq. (11), and alternatively from $d\langle \ln R_\mu \rangle_p / d \ln E$ and $d\langle \ln R_\mu \rangle_{\text{Fe}} / d \ln E$. The three values would be identical if the Heitler model was accurate. Based on the small deviations, we estimate $\sigma_{\text{sys}}[\beta] = 0.02$. By propagating the systematic uncertainty of β , we arrive at a small systematic uncertainty for the predicted logarithmic muon content of $\sigma_{\text{sys}}[\langle \ln R_\mu \rangle] < 0.02$.

With Eqs. (9)–(10), we convert the measured mean depth $\langle X_{\text{max}} \rangle$ into a prediction of the mean logarithmic muon content $\langle \ln R_\mu \rangle$ at $\theta = 67^\circ$ for each hadronic interaction model. The relationship between $\langle X_{\text{max}} \rangle$ and $\langle \ln R_\mu \rangle$ can be represented by a line, which is illustrated in Fig. 5. The Auger measurements at 10^{19} eV are also shown. The discrepancy between data and model predictions is shown by a lack of overlap of the data point with any of the model lines.

The model predictions of $\langle \ln R_\mu \rangle$ and $d\langle \ln R_\mu \rangle / d \ln E$ are summarized and compared to our measurement in Figs. 6–7, respectively. For QGSJETII-03, QGSJETII-04, and EPOS LHC, we use estimated $\langle \ln A \rangle$ data from Ref. [40]. Since QGSJET01 has not been included in that reference, we compute $\langle \ln A \rangle$ using Eq. (9) [4] from the

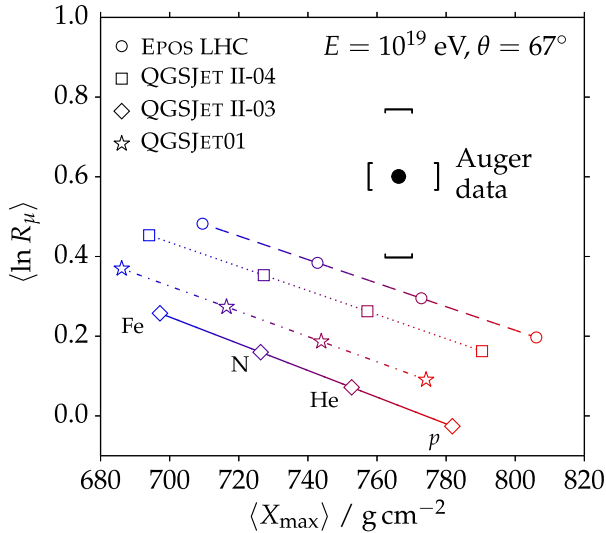


FIG. 5 (color online). Average logarithmic muon content $\langle \ln R_\mu \rangle$ (this study) as a function of the average shower depth $\langle X_{\text{max}} \rangle$ (obtained by interpolating binned data from Ref. [40]) at 10^{19} eV. Model predictions are obtained from showers simulated at $\theta = 67^\circ$. The predictions for proton and iron showers are directly taken from simulations. Values for intermediate masses are computed with the Heitler model described in the text.

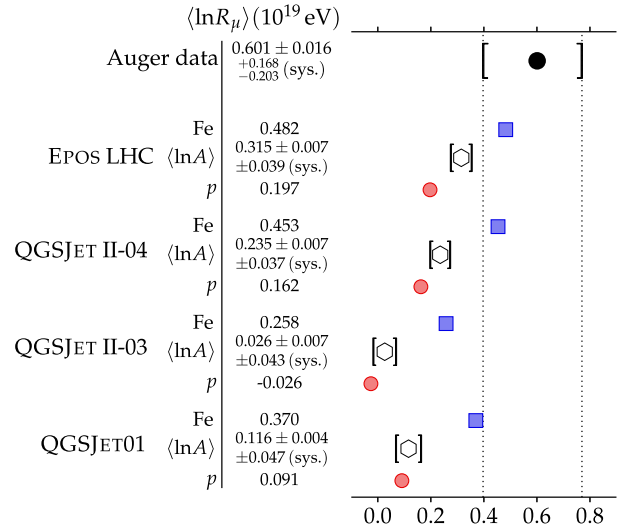


FIG. 6 (color online). Comparison of the mean logarithmic muon content $\langle \ln R_\mu \rangle$ at 10^{19} eV obtained from Auger data with model predictions for proton and iron showers simulated at $\theta = 67^\circ$, and for such mixed showers with a mean logarithmic mass that matches the mean shower depth $\langle X_{\text{max}} \rangle$ measured by the FD. Brackets indicate systematic uncertainties. Dotted lines show the interval obtained by adding systematic and statistical uncertainties in quadrature. The statistical uncertainties for proton and iron showers are negligible and suppressed for clarity.

latest $\langle X_{\text{max}} \rangle$ data [40]. The systematic uncertainty of the $\langle \ln R_\mu \rangle$ predictions is derived by propagating the systematic uncertainty of $\langle \ln A \rangle$ [$\pm 0.03(\text{sys})$], combined with the systematic uncertainty of the Heitler model [$\pm 0.02(\text{sys})$]. The predicted logarithmic gain $d\langle \ln R_\mu \rangle / d \ln E$ is calculated through Eq. (2), while $d \ln A / d \ln E$ is obtained from a straight line fit to $\langle \ln A \rangle$ data points between 4×10^{18} and 5×10^{19} eV. The systematic uncertainty of the $d\langle \ln R_\mu \rangle / d \ln E$ predictions is derived by varying the fitted line within the systematic uncertainty of the $\langle \ln A \rangle$ data [$\pm 0.02(\text{sys})$], and by varying β within its systematic uncertainty in Eq. (2) [$\pm 0.005(\text{sys})$].

The four hadronic interaction models fall short in matching our measurement of the mean logarithmic muon content $\langle \ln R_\mu \rangle$. QGSJETII-04 and EPOS LHC have been updated after the first LHC data. The discrepancy is smaller for these models, and EPOS LHC performs slightly better than QGSJETII-04. Yet none of the models is covered by the total uncertainty interval. The minimum deviation is 1.4σ . To reproduce the higher signal intensity in data, the mean muon number around 10^{19} eV in simulations would have to be increased by 30 to 80% [$^{+17}_{-20}(\text{sys})\%$]. If on the other hand the predictions of the latest models were close to the truth, the Auger energy scale would have to be increased by a similar factor to reach agreement. Without a self-consistent description of air shower observables, conclusions about the mass composition from the measured absolute muon content remain tentative.

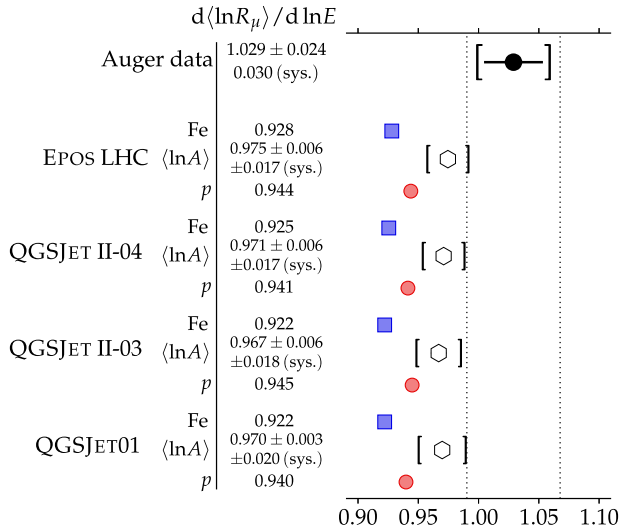


FIG. 7 (color online). Comparison of the logarithmic gain $d\langle \ln R_\mu \rangle / d \ln E$ between 4×10^{18} and 5×10^{19} eV with model predictions in the same style as in Fig. 6.

The situation is better for the logarithmic gain $d\langle \ln R_\mu \rangle / d \ln E$. The measured value is higher than the predictions from $\langle \ln A \rangle$ data, but the discrepancy is smaller. If all statistical and systematic uncertainties are added in quadrature, the deviation between measurement and $\langle \ln A \rangle$ -based predictions is 1.3 to 1.4 σ . The statistical uncertainty is not negligible, which opens the possibility that the apparent deviation is a statistical fluctuation. If we assume that the hadronic interaction models reproduce the logarithmic gain of real showers, which is supported by the internal consistency of the predictions, the large measured value of $d\langle \ln R_\mu \rangle / d \ln E$ disfavors a pure composition hypothesis. If statistical and systematic uncertainties are added in quadrature, we observe deviations from a pure proton (iron) composition of 2.2 σ (2.6 σ).

VI. CONCLUSIONS

We presented the first measurement of the mean muon number in inclined air showers with $\theta > 62^\circ$ between 4×10^{18} and 5×10^{19} eV and its logarithmic gain with energy, based on data from a hybrid detector. We explored the sensitivity of the muon number to the cosmic-ray mass composition and challenged predictions of the muon number from hadronic interaction models. We observe a muon deficit in simulations of 30 to 80% $^{+17}_{-20}$ (sys)% at 10^{19} eV, depending on the model. The estimated deficit takes the mass composition of cosmic rays into account, by comparing our measurement to the average muon number in simulated air showers which match the average depth of shower maximum observed in the data.

Model predictions of the logarithmic gain of muons with rising energy are within the uncertainties compatible with the measured value. The high gain of muons favors a

transition from lighter to heavier elements in the considered energy range. The hypothesis of a constant proton composition, supported by measurements of the depth of shower maximum by the Telescope Array [42] in the northern hemisphere, is disfavored with respect to our result at the level of 2.2 σ .

Our measurement of the muon number combined with measurements of the depth of shower maximum provides important insights into the consistency of hadronic interaction models. The hadronic and muonic components of air showers are less well understood than the electromagnetic component, but all three are physically connected. Improvements in the description of the muonic component will also reduce the systematic uncertainty in the simulation of the other components.

This result is compatible with those of independent studies for showers with $\theta < 60^\circ$ [15], in which different methods have been used to derive the fraction of the signal due to muons at 1000 m from the shower core using the temporal distribution of the signals measured with the SD array.

We have demonstrated how the mass composition of cosmic rays can be inferred from the muon number measured at the ground. To fully explore this potential, the apparent muon deficit in air shower simulations needs to be resolved and the uncertainty of the muon measurement further reduced. The main contributions are the systematic uncertainties in the simulated response of the Auger SD to inclined muons, and the systematic uncertainty in the absolute energy scale. We expect to reduce both of them in the future, which will significantly enhance the constraining power of the muon measurement on the mass composition.

ACKNOWLEDGMENTS

The successful installation, commissioning, and operation of the Pierre Auger Observatory would not have been possible without the strong commitment and effort from the technical and administrative staff in Malargüe. We are very grateful to the following agencies and organizations for financial support: Comisión Nacional de Energía Atómica, Fundación Antorchas, Gobierno De La Provincia de Mendoza, Municipalidad de Malargüe, NDM Holdings and Valle Las Leñas, in gratitude for their continuing cooperation over land access, Argentina; the Australian Research Council; Conselho Nacional de Desenvolvimento Científico e Tecnológico (CNPq), Financiadora de Estudos e Projetos (FINEP), Fundação de Amparo à Pesquisa do Estado de Rio de Janeiro (FAPERJ), São Paulo Research Foundation (FAPESP) Grants No. 2010/07359-6 and No. 1999/05404-3, Ministério de Ciência e Tecnologia (MCT), Brazil; Grants No. MSMT-CR LG13007, No. 7AMB14AR005, No. CZ.1.05/2.1.00/03.0058 and the Czech Science Foundation Grant No. 14-17501S, Czech Republic; Centre de Calcul Grant No. IN2P3/

CNRS, Centre National de la Recherche Scientifique (CNRS), Conseil Régional Ile-de-France, Département Physique Nucléaire et Corpusculaire (Grant No. PNC-IN2P3/CNRS), Département Sciences de l'Univers (Grant No. SDU-INSU/CNRS), Institut Lagrange de Paris, Grant No. ILP LABEX ANR-10-LABX-63, within the Investissements d'Avenir Programme Grant No. ANR-11-IDEX-0004-02, France; Bundesministerium für Bildung und Forschung (BMBF), Deutsche Forschungsgemeinschaft (DFG), Finanzministerium Baden-Württemberg, Helmholtz-Gemeinschaft Deutscher Forschungszentren (HGF), Ministerium für Wissenschaft und Forschung, Nordrhein Westfalen, Ministerium für Wissenschaft, Forschung und Kunst, Baden-Württemberg, Germany; Istituto Nazionale di Fisica Nucleare (INFN), Ministero dell'Istruzione, dell'Università e della Ricerca (MIUR), Gran Sasso Center for Astroparticle Physics (CFA), CETEMPS Center of Excellence, Italy; Consejo Nacional de Ciencia y Tecnología (CONACYT), Mexico; Ministerie van Onderwijs, Cultuur en Wetenschap, Nederlandse Organisatie voor Wetenschappelijk Onderzoek (NWO), Stichting voor Fundamenteel Onderzoek der Materie (FOM), Netherlands; National Centre for Research and Development, Grants No. ERA-NET-ASPERA/01/11 and No. ERA-NET-ASPERA/02/11, National Science Centre,

Grants No. 2013/08/M/ST9/00322, No. 2013/08/M/ST9/00728 and No. HARMONIA 5 - 2013/10/M/ST9/00062, Poland; Portuguese national funds and FEDER funds within COMPETE—Programa Operacional Factores de Competitividade through Fundação para a Ciência e a Tecnologia, Portugal; Romanian Authority for Scientific Research ANCS, Grants No. CNDI-UEFISCDI, No. 20/2012 and No. 194/2012, No. 1/ASPERA2/2012 ERA-NET, No. PN-II-RU-PD-2011-3-0145-17, and No. PN-II-RU-PD-2011-3-0062, the Minister of National Education, Programme for research—Space Technology and Advanced Research—STAR, Grant No. 83/2013, Romania; Slovenian Research Agency, Slovenia; Comunidad de Madrid, FEDER funds, Ministerio de Educación y Ciencia, Xunta de Galicia, European Community 7th Framework Program, Grant No. FP7-PEOPLE-2012-IEF-328826, Spain; Science and Technology Facilities Council, United Kingdom; Department of Energy, Contracts No. DE-AC02-07CH11359, No. DE-FR02-04ER41300, No. DE-FG02-99ER41107 and No. DE-SC0011689, National Science Foundation, Grant No. 0450696, The Grainger Foundation, USA; NAFOSTED, Vietnam; Marie Curie-IRSES/EPLANET, European Particle Physics Latin American Network, European Union 7th Framework Program, Grant No. PIRSES-2009-GA-246806; and UNESCO.

-
- [1] J. Abraham *et al.* (Pierre Auger Collaboration), *Science* **318**, 938 (2007).
- [2] P. Abreu *et al.* (Pierre Auger Collaboration), *Astropart. Phys.* **34**, 314 (2010).
- [3] J. Abraham *et al.* (Pierre Auger Collaboration), *Phys. Lett. B* **685**, 239 (2010).
- [4] P. Abreu *et al.* (Pierre Auger Collaboration), *J. Cosmol. Astropart. Phys.* 02 (2013) 026.
- [5] K. Kampert and M. Unger, *Astropart. Phys.* **35**, 660 (2012).
- [6] J. Matthews, *Astropart. Phys.* **22**, 387 (2005).
- [7] T. Pierog and K. Werner, *Phys. Rev. Lett.* **101**, 171101 (2008).
- [8] R. Ulrich, R. Engel, and M. Unger, *Phys. Rev. D* **83**, 054026 (2011).
- [9] J. Abraham *et al.* (Pierre Auger Collaboration), *Nucl. Instrum. Methods Phys. Res., Sect. A* **523**, 50 (2004).
- [10] J. Abraham *et al.* (Pierre Auger Collaboration), *Nucl. Instrum. Methods Phys. Res., Sect. A* **613**, 29 (2010).
- [11] J. Abraham *et al.* (Pierre Auger Collaboration), *Nucl. Instrum. Methods Phys. Res., Sect. A* **620**, 227 (2010).
- [12] J. Abraham *et al.* (Pierre Auger Collaboration), *Phys. Rev. Lett.* **100**, 211101 (2008).
- [13] J. Abraham *et al.* (Pierre Auger Collaboration), *Phys. Rev. D* **79**, 102001 (2009).
- [14] M. Ave, J. A. Hinton, R. A. Vázquez, A. A. Watson, and E. Zas, *Astropart. Phys.* **18**, 367 (2003).
- [15] B. Kégl *et al.* (Pierre Auger Collaboration), in *The Pierre Auger Observatory: Contributions to the 33rd International Cosmic Ray Conference, Rio de Janeiro, Brazil, 2013*, arXiv:1107.4809.
- [16] G. Farrar *et al.* (Pierre Auger Collaboration), *The Pierre Auger Observatory: Contributions to the 33rd International Cosmic Ray Conference, Rio de Janeiro, Brazil, 2013*, arXiv:1307.5059.
- [17] A. Aab *et al.* (Pierre Auger Collaboration), *Phys. Rev. D* **90**, 012012 (2014).
- [18] M. Ave, R. A. Vázquez, E. Zas, J. A. Hinton, and A. A. Watson, *Astropart. Phys.* **14**, 109 (2000).
- [19] I. Valiño *et al.* (Pierre Auger Collaboration), *The Pierre Auger Observatory: Contributions to the 33rd International Cosmic Ray Conference, Rio de Janeiro, Brazil, 2013*, arXiv:1307.5059.
- [20] M. Ave, J. Hinton, R. Vázquez, A. Watson, and E. Zas, *Phys. Rev. Lett.* **85**, 2244 (2000).
- [21] H. P. Dembinski (Pierre Auger Collaboration), *The Pierre Auger Observatory I: The Cosmic Ray Energy Spectrum and Related Measurements, Beijing, China, 2011*, arXiv:1107.4809.
- [22] R. A. Vázquez (Pierre Auger Collaboration), *The Cosmic Ray Energy Spectrum and Related Measurements with the Pierre Auger Observatory*, arXiv:0906.2189.

- [23] G. Rodriguez (Pierre Auger Collaboration), [arXiv:1107.4809](#).
- [24] S. S. Ostapchenko, *Nucl. Phys. B, Proc. Suppl.* **151**, 143 (2006).
- [25] M. Ave, R. A. Vázquez, and E. Zas, *Astropart. Phys.* **14**, 91 (2000).
- [26] H. P. Dembinski, P. Billoir, O. Deligny, and T. Hebbeker, *Astropart. Phys.* **34**, 128 (2010).
- [27] J. Allison *et al.*, *IEEE Trans. Nucl. Sci.* **53**, 270 (2006).
- [28] S. Argirò, S. L. C. Barroso, J. Gonzalez, L. Nellen, T. Paul, T. A. Porter, L. Prado, Jr., M. Roth, R. Ulrich, D. Veberič, *Nucl. Instrum. Methods Phys. Res., Sect. A* **580**, 1485 (2007).
- [29] I. Valiño, J. Alvarez-Muñiz, M. Roth, R. A. Vazquez, and E. Zas, *Astropart. Phys.* **32**, 304 (2010).
- [30] A. Aab *et al.* (Pierre Auger Collaboration), *J. Cosmol. Astropart. Phys.* **08** (2014) 019.
- [31] S. J. Sciutto, *Proceedings of ICRC 2001: The AIREs system for air shower simulations*, [arXiv:astro-ph/0106044v1](#).
- [32] N. N. Kalmykov and S. S. Ostapchenko, *Yad. Fiz.* **56N3**, 105 (1993) [*Phys. At. Nucl.* **56**, 346 (1993)].
- [33] D. Heck, G. Schatz, T. Thouw, J. Knapp, and J. N. Capdevielle, Report No. FZKA 6019, 1998.
- [34] S. S. Ostapchenko, *Phys. Rev. D* **83**, 014018 (2011).
- [35] T. Pierog, Iu. Karpenko, J. M. Katzy, E. Yatsenko, and K. Werner, Report No. DESY-13-125, 2013.
- [36] National Imagery and Mapping Agency, Report No. TR 8350.2, U.S. Department of Defense, 1997.
- [37] P. Ghia *et al.* (Pierre Auger Collaboration), in *Proceedings 30th International Cosmic Ray Conference, Mérida, Mexico, 2007* (2007), pp. 315–318.
- [38] V. Verzi *et al.* (Pierre Auger Collaboration), in *Proceedings 33rd International Cosmic Ray Conference, Rio de Janeiro, Brazil, 2013* (2013), [arXiv:1307.5059](#).
- [39] R. Pesce *et al.* (Pierre Auger Collaboration), *Proceedings 32nd International Cosmic Ray Conference, Beijing, China, 2011* (2011), [arXiv:1107.4809](#).
- [40] A. Letessier-Selvon *et al.* (Pierre Auger Collaboration), in *Proceedings 33rd International Cosmic Ray Conference, Rio de Janeiro, Brazil, 2013* (2013), [arXiv:1310.4620](#).
- [41] E.-J. Ahn *et al.* (Pierre Auger Collaboration), in *Proceedings 33rd International Cosmic Ray Conference, Rio de Janeiro, Brazil, 2013* (2013), [arXiv:1307.5059](#).
- [42] M. Allen *et al.* (Telescope Array Collaboration), in *Proceedings 33rd International Cosmic Ray Conference, Rio de Janeiro, Brazil, 2013* (2013).